Surface & Coatings Technology 232 (2013) 804–813

Contents lists available at ScienceDirect

Surface & Coatings Technology

journal homepage: www.elsevier.com/locate/surfcoat

Growth of TiO_2/Cu films by HiPIMS for accelerated bacterial loss of viability ☆

Sami Rtimi [a], Oualid Baghriche [a], Cesar Pulgarin [a,**], Jean-Claude Lavanchy [b], John Kiwi [c,*]

[a] Ecole Polytechnique Fédérale de Lausanne, EPFL-SB-ISIC-GPAO, Station 6, CH-1015 Lausanne, Switzerland
[b] Université de Lausanne, IMG, Centre d'Analyse Minérale, Bat Anthropole, CH-1015 Lausanne, Switzerland
[c] Ecole Polytechnique Fédérale de Lausanne, EPFL-SB-ISIC-LPI, Bat Chimie, Station 6, CH1015 Lausanne, Switzerland

ARTICLE INFO

Article history:
Received 23 February 2013
Accepted in revised form 23 June 2013
Available online 1 July 2013

Keywords:
HIPIMS sputtering
Nano-composite layers
E. coli viability
Coating thickness
Metal savings
ICP-MS

ABSTRACT

This study shows the first complete report on ultrathin TiO_2/Cu nano-particulate films sputtered by highly ionized pulsed plasma magnetron sputtering (HIPIMS) leading to fast bacterial loss of viability. The Cu- and the TiO_2/Cu sputtered films induced complete *Escherichia coli* inactivation in the dark, which was not observed in the case of TiO_2. When Cu was present, the bacterial inactivation was accelerated under low intensity solar simulated light and this has implications for a potential for a practical technology. The design, preparation, testing and surface characterization of these innovative films are described in this study. The HIPIMS sputtered composite films present an appreciable savings in metals compared to films obtained by conventional sputtering methods. HIPIMS sputtering induces a strong interaction with the rugous polyester 3-D structure due to the higher fraction of the Cu-ions (M^+) attained in the magnetron chamber. The Cu-leaching during the bacterial inactivation was monitored by ion-coupled plasma mass spectrometry (ICP-MS) and found to be in the ppb range. The amounts found were below the cytotoxicity level allowed by the standards related to human health. The immiscibility of Cu and TiO_2 in the TiO_2/Cu films is shown by High Angular Dark Field (HAADF) microscopy. A mechanism for the photo-induced interfacial charge transfer (IFCT) between TiO_2 and Cu is suggested.

1. Introduction

Antimicrobial surfaces can reduce/eliminate hospital-acquired infections (HAI) acquired on contact with bacteria surviving for long times in hospital facilities [1,2]. To preclude/decrease viral, nosocomial infections and antibiotic resistant bacteria Borkow and Gabbay [3] introduced Cu into textile fabrics. Sunada et al. [4,5], Torres et al. [6a], O. Akhavan [6b–d] and others [6e–i] have recently reported the preparation of the Cu and TiO_2/Cu films by sol–gel methods with materials absorbing in the visible range. These sol–gel deposited films are not mechanically stable, in many cases their preparation is not reproducible, do not present uniformity but only low adhesion since they can be wiped off by a cloth or thumb [7]. Films obtained by direct current magnetron sputtering (DC/DCP) as reported avoid the disadvantages of Cu-films prepared by sol–gel methods [4–7] since they deposit uniform and adhesive metal film chemical bonding and mechanical interlocking leading to substrates resisting up to 120–130 °C.

In recent years physical vapor deposition (PVD) has been used to produce antimicrobial films by condensation of a vaporized precursor onto the substrate at relatively high temperatures. Page et al. [8], Foster et al. [9], Dunlop et al. [10] and Page et al. [11] have reported antibacterial film preparation of Ag and Cu films on glass and thin polymer films by PVD. TiO_2, Ag, and Cu films 6 to 50 nm thick have been shown to inactivate bacteria under UV and in some cases under visible light irradiation. The disadvantages of the PVD deposition approach are the high investment costs, the high temperatures needed precluding film deposition on textiles besides the large amount of heat used requiring costly cooling systems. High power impulse magnetron sputtering (HIPIMS) has been used more recently to prepare films by applying strong electrical pulses leading to sputter layers presenting superior resistance against corrosion and oxidation [12,13]. The non-uniform deposition on rugous and complex shape substrates is one of the main problems encountered when depositing uniform Cu-films by direct current pulsed magnetron sputtering (DC/DCP) [13].

We address in this study HIPIMS sputtering on 3-D substrates leading to ultrathin uniform films showing an accelerated bacterial deactivation due to the induced high energy Cu-ions (M^+) produced in the magnetron chamber, the HIPIMS plasma density and the increased effect of the applied bias voltage on the Cu-ions (M^+) sputtered by HIPIMS compared to DC/DCP sputtering. We present hereby a study on Cu and TiO_2/Cu films sputtered by HIPIMS describing the deposition parameters, the loss of bacterial viability under light and a detailed surface characterization. The results obtained will be compared to Cu and Cu/TiO_2 layers sputtered

* Corresponding author. Tel.: +41 21 693 5160; fax: +41 21 693 5690.
** Corresponding author. Tel.: +41 21 693 47 20; fax: +41 21 693 6161.
E-mail addresses: cesar.pulgarin@epfl.ch (C. Pulgarin), john.kiwi@epfl.ch (J. Kiwi).

0257-8972/$ – see front matter © 2013 The Authors. Published by Elsevier B.V. All rights reserved.
http://dx.doi.org/10.1016/j.surfcoat.2013.06.102

by DC and DCP-magnetron sputtering during the last three years [14–17]. The levels of contamination in UK hospitals have been reported to be ~10^5 CFU/cm^2 in diabetic wound dressing room and in hospital residence rooms a density of 10^2 CFU/cm^2 only was found. The TiO_2/Cu polyester samples described in this study present the potential to be practical candidates to avoid biofilm formation and disinfect hospital rooms not involving a high level of bacterial concentration [1–5].

2. Experimental section

2.1. Sputtering parameters, film thickness, sample composition and determination of the Cu and Ti by ICP-MS during bacterial inactivation

HIPIMS deposition of Ti and Cu was carried out in a CMS-18 Vacuum system from Kurt Lesker Ltd. evacuated to 5.8×10^{-3} mbar by a turbomolecular pump. The Cu- as well as the TiO_2 target were 50 mm in diameter, 99.99% pure from K. Lesker Ltd., UK. The TiO_2/Cu target was 2 in. in diameter and had a composition of 60/40 at.% in TiO_2 and Cu respectively. The HIPIMS was operated at 500 Hz with pulses of 100 μs separated by 1.9 ms, leading to a deposition rate for TiO_2/Cu of 15.3 nm/min. The average power was 87.5 W (5 A × 350 V) and the power per pulse of 100 μs was 1750 W. The 5 A current is the current at one pulse, the voltage at one pulse is 350 V and the pulses had a rectangular shape since the pulse duration was 100 μs with an off-period of 1900 μs.

In the case of DCP, 622 V and 0.3 A were applied during the 3 pulses of 10 μs each within a 50 microsecond period. This gives 187 W per period or 62.3 W/pulse and an average power of 312 W/period.

The polyester used corresponds to the EMPA test cloth sample No 407. It is a polyester Dacron polyethylene terephthalate, type 54 spun, 130 μm thick plain weave ISO 105-F04 used for color fastness determinations.

The calibration of the Cu-nanoparticulate film thickness by HIPIMS on the Si-wafers is shown in Fig. 1A. The film thickness was determined with a profilometer (Alphastep500, TENCOR). The X-ray fluorescence (XRF) determination of the Ti/Cu samples was evaluated in a PANalytical PW2400 spectrometer.

Inductively coupled plasma spectrometry (ICP-MS) was used to determine the Cu since it is a sensitive analytical technique because due to the low background and high ion transmission. The Finnigan™ ICPS used was equipped with a double focusing reverse geometry mass spectrometer able of a resolution of 1.2×10^5 cps/ppb, and a detection limit of 0.2 ng/L. 1 cm^2 samples were placed in Eppendorf tubes containing 1 ml NaCl/KCl 0.08% solution. The solutions were then diluted 10 times to reach the volume necessary for the ICP-MS analyses.

2.2. Escherichia coli loss of viability evaluation

The samples of *Escherichia coli* (*E. coli* K12) were obtained from the Deutsche Sammlung von Mikro-organismen und Zellkulturen GmbH (DSMZ) ATCC23716, Braunschweig, Germany to test the antibacterial activity of the Cu-polyester fabrics according to a previous work reported by our laboratory [17a,b]. The bacterial counting data reported were replicated three times. To verify that no re-growth of *E. coli* occurs after the total inactivation observed in the first disinfection cycle, the samples were incubated for 24 h at 37 °C. Then bacterial suspension of 100 μl was deposited on 3 Petri dishes to obtain replicates of the bacterial counting. These samples are incubated at 37 °C for 24 h. No bacterial re-growth was observed. Samples were irradiated in the cavity of a Suntest solar simulator with a light dose of 50 mW/cm^2. The statistical analysis of the results was performed for the decrease of the bacterial CFU values reporting the standard deviation values for the runs showing the fastest bacterial inactivation. The average values were compared by one-way analysis of variance and with the value of statistical significance.

2.3. Diffuse reflectance spectroscopy (DRS), electron microscopy (TEM, HAADF) and XRD of samples

Diffuse reflectance spectroscopy was carried out using a Perkin Elmer Lambda 900 UV–VIS–NIR spectrometer provided for with a PELA-1000 accessory within the wavelength range of 200–800 nm and a resolution of 1.0 nm. The absorption of the samples was plotted in Kubelka–Munk (KM) arbitrary unit vs wavelength. Irradiation of the samples was carried out in a tubular cavity of a Suntest Hereaus GmbH solar simulator, Hanau, Germany.

Transmission electron microscopy was carried out in a Philips CM-12 (field emission gun, 300 kV, 0.17 nm resolution) microscope at 120 kV to measure grain size of the TiO_2/Cu films. The textiles were embedded in epoxy resin 45359 Fluka and the fabrics were cross-sectioned with an ultramicrotome (Ultracut E) and at a knife angle at 35°. High-Angle Annular Dark-Field (HAADF) imaging was used to map the scanning electron microscopy (STEM). These images (Z-contrast images) are obtained by collecting the scattered electrons passing through the objective provided with an annular dark-field detector.

Crystal structures were characterized by X-ray diffraction (XRD) and recorded on an X'Pert MPD PRO from PANalytical equipped with a secondary graphite (002) monochromator and an X'Celerator detector operated in Bragg–Brentano geometry. A step size of 0.0081 was chosen and an acquisition time of 2 min per degree.

2.4. X-ray photoelectron spectroscopy (XPS) and detection of highly oxidative radicals in the sputtered samples

An AXIS NOVA photoelectron spectrometer (Kratos Analytical, Manchester, UK) equipped with monochromatic AlK_α ($h\nu$ = 1486.6 eV) anode was used during the study. The electrostatic charge effects on the samples were compensated by means of the low-energy electron source working in combination with a magnetic immersion lens. The carbon C1s line with position at 284.6 eV was used as a reference to correct for charging effects. The XPS spectra for the Cu-species were analyzed by means of spectra deconvolution software (CasaXPS-Vision 2, Kratos Analytical UK). The percentage surface atomic concentration of some elements was determined by fitting of the peak areas using known sensitivity factors [18a]. Spectrum background was subtracted according to the Shirley subtraction GL(30) program attached to the Kratos unit [18b].

The detection of the oxidative species (mainly OH-radicals) in the TiO_2/Cu sputtered samples was carried out according to Ishibashi et al. [19]. Terephthalic acid 99% was an ACROSS reagent. The fluorescence spectrum of the 2-hydroxyterephthalic acid generated by the reaction of terephthalic acid with OH was measured on a Perkin Elmer LS-50B fluorescence spectrometer.

3. Results and discussion

3.1. Sample film thickness bacterial loss of viability, diffuse reflectance spectroscopy (DRS) and determination of elusive Cu

Fig. 1A shows the results of the thickness calibration for HIPIMS sputtered Si-wafers at 5 A for Cu, TiO_2 and TiO_2/Cu 60%/40% target. The fastest bacterial inactivation leading to complete inactivation was observed when the polyester sputtered for 150 s with the TiO_2/Cu target (Fig. 1B) depositing a composite film 38 nm thick. This is equivalent to ~190 layers, 0.2 nm thick with 10^{15} atoms/cm^2 and deposited at a rate of 15.3 nm/min or 7.6×10^{16} atoms/cm^2/min. X-ray fluorescence in Table 1 shows the content of TiO_2 and CuO with increased sputtering time. When using the TiO_2/CuO 60%/40% target a ratio of TiO_2/CuO of 4–5 times was observed for the different sputtering times.

The bacterial loss of viability in Fig. 1B, trace 6 shows that no bacterial loss of viability occurs on polyester alone under light irradiation. Samples sputtered for 150 s induced a slow loss of bacterial viability

within 120 min in the dark. Under actinic light radiation, traces 3 and 4 indicate that sputtering times of 30 s and 60 s induce faster bacterial loss of viability kinetics. A sputtering time of 150 s induced the shortest inactivation time (trace 1). Sputtering for 300 s induce bacterial inactivation taking longer times compared to samples sputtered for 150 s. Therefore, the amount of Cu^0 is not the main species leading to bacterial inactivation. A sputtering time of 150 s is seen to lead to the most favorable structure-reactivity for the Cu-polyester leading to the shortest *E. coli* inactivation. This sample presents the highest amount of Cu-sites held in exposed positions interacting on the surface or close to the polyester surface with *E. coli* leading to bacterial loss of viability [17a]. The surface bactericide action seems to be due to a synergic effect introduced by the TiO_2/Cu layers since longer times were observed when sputtering TiO_2 as shown next in Fig. 1C.

Fig. 1C shows the bacterial inactivation kinetics by the HIPIMS TiO_2 sputtered samples. As shown in Fig. 1C no bacterial inactivation takes place in the dark but the bacterial inactivation becomes faster for HIPIMS sputtering times between 1 min (trace 5) and 4 min (trace 2). Longer deposition times between 10 and 30 min did not accelerate the loss of viability kinetics due to the fact that an increased TiO_2 thickness >12 nm sputtered within 4 min leads to: a) bulk inward diffusion of the charge carriers generated on TiO_2 under light leading to highly oxidative radicals [20,21], and b) longer sputtering times which facilitate the TiO_2 inter-particle growth decreasing the TiO_2 contact surface with bacteria [14,15]. The TiO_2 bactericide inactivation mechanism has been reported and will not be discussed further in this study [6,7,20]. Fig. 1D shows the *E. coli* inactivation within 60 min for HIPIMS Cu-sputtered samples within 15, 30, and 60s. This inactivation time is longer than the time reported in Fig. 1B suggesting a synergic effect between TiO_2 and Cu leading to a faster loss of viability.

Fig. 1E presents the results for the diffuse reflectance spectroscopy (DRS) for the TiO_2/Cu samples used to evaluate the bacterial inactivation (Fig. 1B). The absorption in Kubelka–Munk units shows an agreement with the data reported for TiO_2 and Cu in Table 1, showing that TiO_2 is the main surface element. The $Cu/Cu_2O/CuO$ absorption increases with longer Cu-sputtering times up to 300 s [22]. The weak absorption from 400 to 500 is due to the interfacial charge transfer (IFTC) from the TiO_2 to CuO. The optical absorption between 500 and 600 nm is due to the

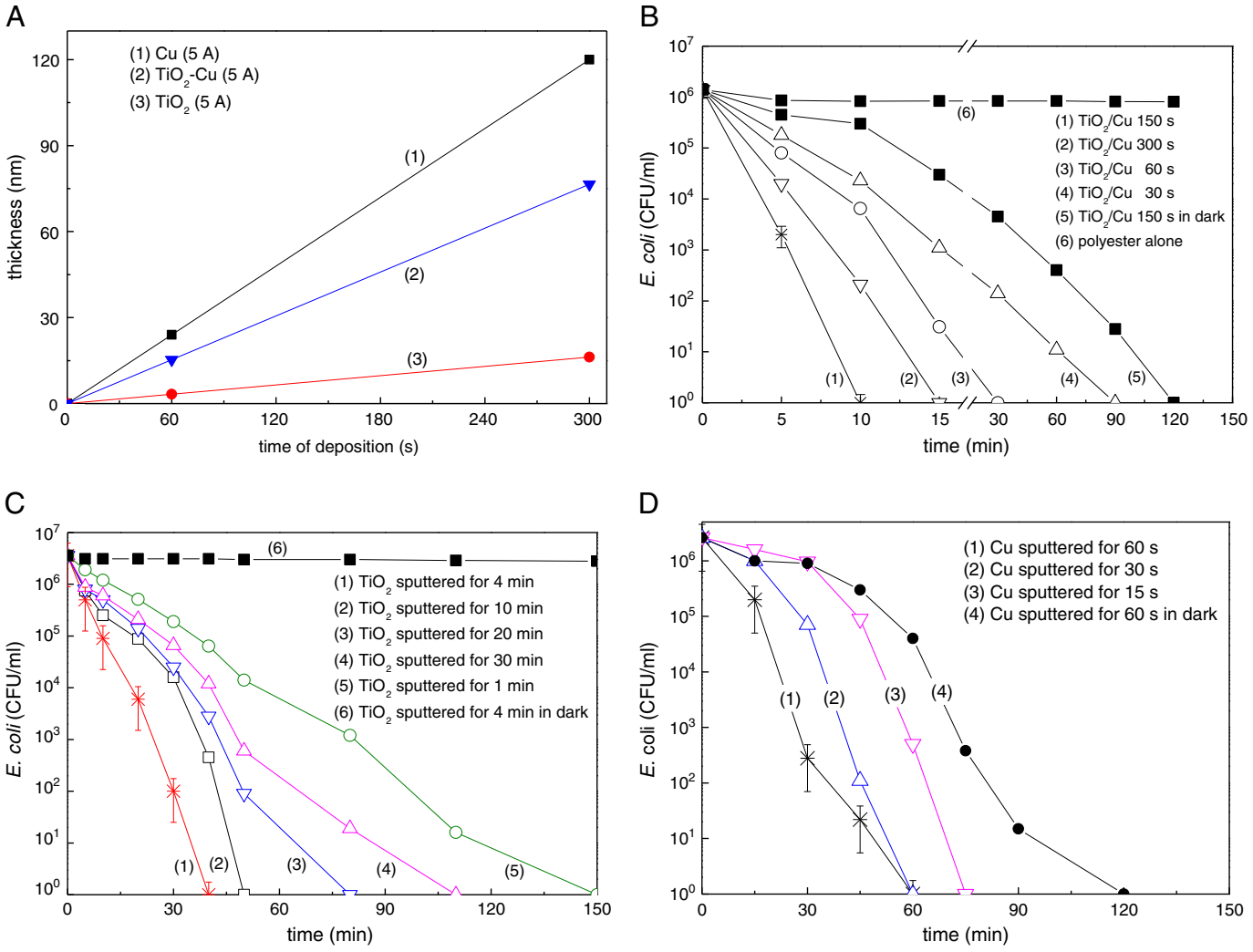

Fig. 1. A. Thickness calibration of: (1) Cu, (2) TiO_2–Cu and (3) TiO_2 HIPIMS-sputtered under current intensity of 5 A. B. *E. coli* survival on TiO_2/Cu HIPIMS-sputtered on polyester for different times in the dark and under Osram Lumilux 18 W/827 actinic lamp (4 mW/cm^2). C. *E. coli* survival on TiO_2 HIPIMS-sputtered (5 A) on polyester for different times in the dark and under Osram Lumilux 18 W/827 actinic lamp (4 mW/cm^2). D. *E. coli* survival on Cu HIPIMS-sputtered for different times in the dark and under Osram Lumilux 18 W/827 actinic lamp (4 mW/cm^2). E. DRS of TiO_2/Cu polyester samples sputtered by HIPIMS for different times with 5 A (90 W). F. *E. coli* survival on TiO_2/Cu HIPIMS-sputtered samples for 150 s under different light intensities by an Osram Lumilux 18 W/827 actinic lamp. G. *E. coli* survival on TiO_2/Cu HIPIMS-sputtered sample for 150 s under an Osram Lumilux 18 W/827 actinic lamp (4 mW/cm^2) up to the 8th repetitive cycle. H. Concentration of ions eluted into the solution determined by ICP-MS up to the 8th recycling of TiO_2/Cu samples inactivating *E. coli* K-12 under solar simulated light irradiation.

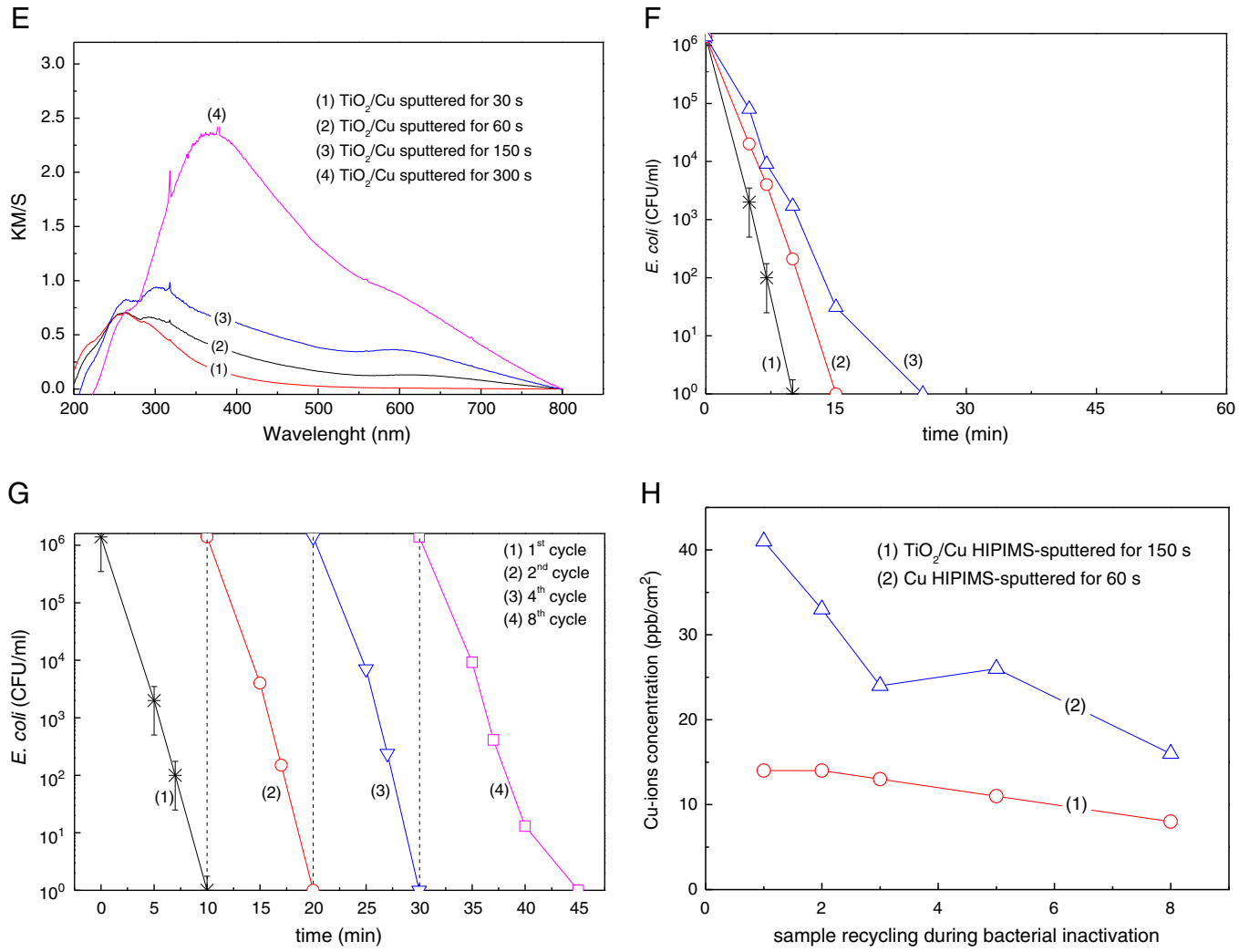

Fig. 1 (*continued*).

interband transition of Cu_2O. The absorption between 600 and 800 nm has been attributed to the exciton band and the CU (II) d–d transition.

The rough UV–vis reflectance data cannot be used directly to assess the absorption coefficient of the sputtered polyester because of the large scattering contribution to the reflectance spectra. Normally, a weak dependence is assumed for the scattering coefficient S on the wavelength. The KM/S values for the samples in Fig. 1E are proportional to the TiO_2/Cu absorption coefficient up to sputtering times of 150 s and these values are in agreement with the trend observed for the inactivation kinetics reported (Fig. 1B).

Fig. 1F shows the loss of bacterial viability due to the TiO_2/Cu sample irradiated by three different light doses in the solar simulator. The loss of bacterial viability with time in Fig. 1F is shown to be a function of the intensity of the applied visible light. The mechanism will be discussed below in the section describing the results presented in Fig. 4.

Fig. 1G shows the recycling of the TiO_2/Cu (150 s) sample up to the 8th cycle. No loss in activity was observed in the sample during the sample recycling. The sample was thoroughly washed after each recycling run leading to the reuse of the sample since complete bacterial loss of viability was attained after each cycle. The chemical state and environment of the CuO/Cu-ions seem not to change after the bacterial loss of viability showing the stable nature of the TiO_2/Cu on the polyester fabric.

Fig. 1H shows the release of Cu-ions inactivating *E. coli* as a function of catalyst recycling. Fig. 1H shows the repetitive release of Cu-ions up to the 8th recycling as measured by ICP-MS. The release of Cu- from the TiO_2/Cu samples shown in Fig. 1H was ~8 ppb/cm^2. This value is lower compared to the Cu-release from the Cu-sputtered samples reaching up to ~18 ppb Cu/cm^2 at the end of the 8th cycle. In both cases the small amounts of Cu are considered not to be cytotoxic to *mammalian* cells and proceed through an oligodynamic effect [6,17]. The Cu and TiO_2/Cu induced bacterial inactivation is carried out in a way that it is not toxic to human health.

Table 1
TiO_2 and Cu loadings determined by X-ray fluorescence for the HIPIMS sputtered polyester samples used in this study.

Samples	wt.% CuO/wt polyster	wt.% TiO_2/wt polyester	Current intensity
TiO_2 (30 min)	–	0.513	5 A
TiO_2 (20 min)	–	0.382	
TiO_2 (10 min)	–	0.192	
TiO_2 (4 min)	–	0.042	
TiO_2 (1 min)	–	0.039	
TiO_2 (30 s)	–	0.025	
Cu (60 min)	0.340	–	5 A
Cu (30 s)	0.189	–	
Cu (15 s)	0.144	–	
TiO_2/Cu (300 s)	0.107	0.570	5 A
TiO_2/Cu (150 s)	0.088	0.446	
TiO_2/Cu (60 s)	0.063	0.317	
TiO_2/Cu (30 s)	0.060	0.243	

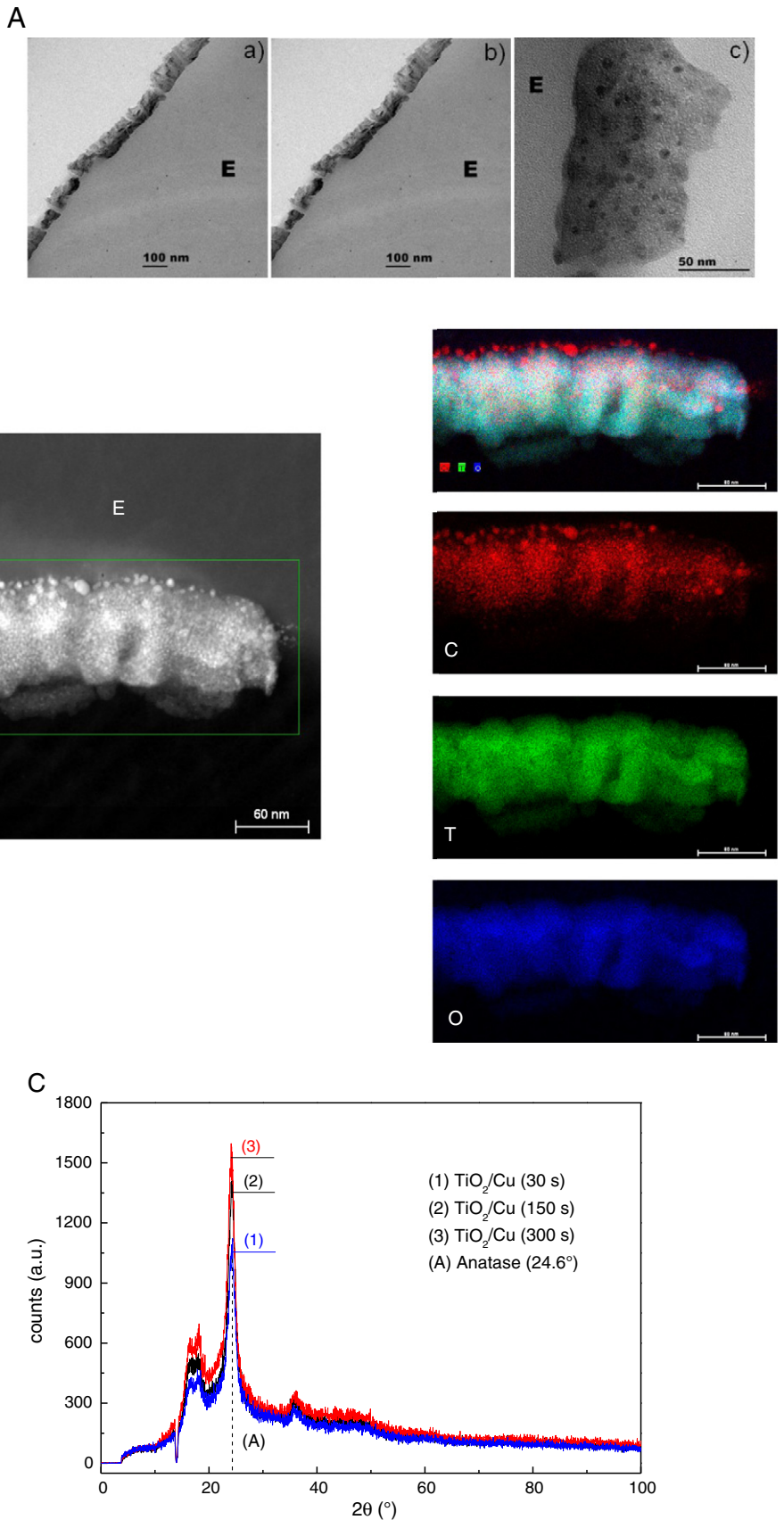

Fig. 2. A. Transmission electron microscopy (TEM) of: a) Cu sputtered for 150 s by HIPIMS on polyester, b) TiO_2/Cu sputtered for 30 s by HIPIMS on polyester and c) TiO_2/Cu sputtered for 150 s polyester. B. High-Angle Annular Dark-Field imaging (HAADF) images of TiO_2/Cu HIPIMS sputtered for 150 s showing the complete sample and the mapping of Cu, Ti and O by Z-contrast imaging in the TEM image of the sample. C. XRD patterns for Cu/CuO/TiO_2 and TiO_2 anatase highly crystallized films sputtered on polyester by HIPIMS at different times. Due to the Cu-loading <0.1%, the Cu is not detected by the XRD and only the sharp anatase peak at the 2θ angle of 24.60 is shown in the XRD spectrogram.

Table 2
Percentage surface atomic concentration of TiO_2/Cu (150 s) HIPIMS film as a function of bacterial inactivation time under simulated solar irradiation.

Samples	C	O	N	S	Ti	Cu
TiO_2/Cu (150 s) at time zero	52.63	30.00	0.00	0.00	4.75	9.61
TiO_2/Cu (150 s) contacted with bacteria at time zero	54.21	31.02	0.09	0.00	5.71	10.97
TiO_2/Cu (150 s) at 5 min of bacterial inactivation	55.19	31.88	0.10	0.03	5.55	9.99
TiO_2/Cu (150 s) at 10 min of bacterial inactivation	53.04	30.57	0.06	0.00	5.57	10.02
TiO_2/Cu (150 s) at 15 min of bacterial inactivation	53.07	30.98	0.04	0.00	5.55	10.00

3.2. Steric factors and electron microscopy (TEM) and sample XRD

The particle size of the film nanoparticulate and the hydrophobic–hydrophilic balance determine to a great extent the surface photocatalytic properties. Samples sputtered for 30 s show Cu-nanoparticles between 8 and 15 nm. The TiO_2 samples sputtered for 150 s present sizes between 8 and 12 nm, and the TiO_2/Cu samples sputtered for 150 s presented particles 5–10 nm. The TiO_2 binds, disperses and stabilizes the Cu-clusters on the polyester surfaces. The nanoparticles' small size accounts partly for the favorable bacterial inactivation kinetics due to the large surface area per unit mass [14,15,20,23]. The distribution of TiO_2 and Cu-nanoparticles on the polyester was found to be uniform not presenting any cracks. The uniformity of the film is beneficial for the bacterial adhesion which is a primary step leading to bacterial loss of viability to proceed favorably [1,2,8]. The electronic transfer between the TiO_2/Cu sample and the *E. coli* depends on the length of the charge diffusion in the composite film. This in turn is a function of the TiO_2 and Cu particle size and shape [20,21].

The interfacial distances between TiO_2 and Cu/CuO on the polyester surface range from below 5 nm and up. This allows the interfacial charge transfer (IFCT) to proceed with a high quanta efficiency [20,23]. Quantum size effects have been shown to occur in particles with sizes of 10 nm having about 10^4 atoms as presented by the TiO_2 particles with sizes of ~10 nm [23,24]. But in the CuO nanoparticles the charge recombination increases take place within shorter times due to the decrease in the available space for charge separation. Also, the decrease of the space charge layer decreases further the potential depth.

Fig. 2B presents in the left hand side TiO_2/Cu microscopy contrasted by high angular annular dark field (HAADF) showing the Cu-nanoparticles to be immiscible with Ti. Cu^{2+} does not substitute Ti^{4+} in the TiO_2 lattice because of the significant difference in the *radii* of Ti^{4+} (0.53 Å) and Cu^{2+} (1.28 Å). The right hand side insets show the mapping of the Cu, Ti and

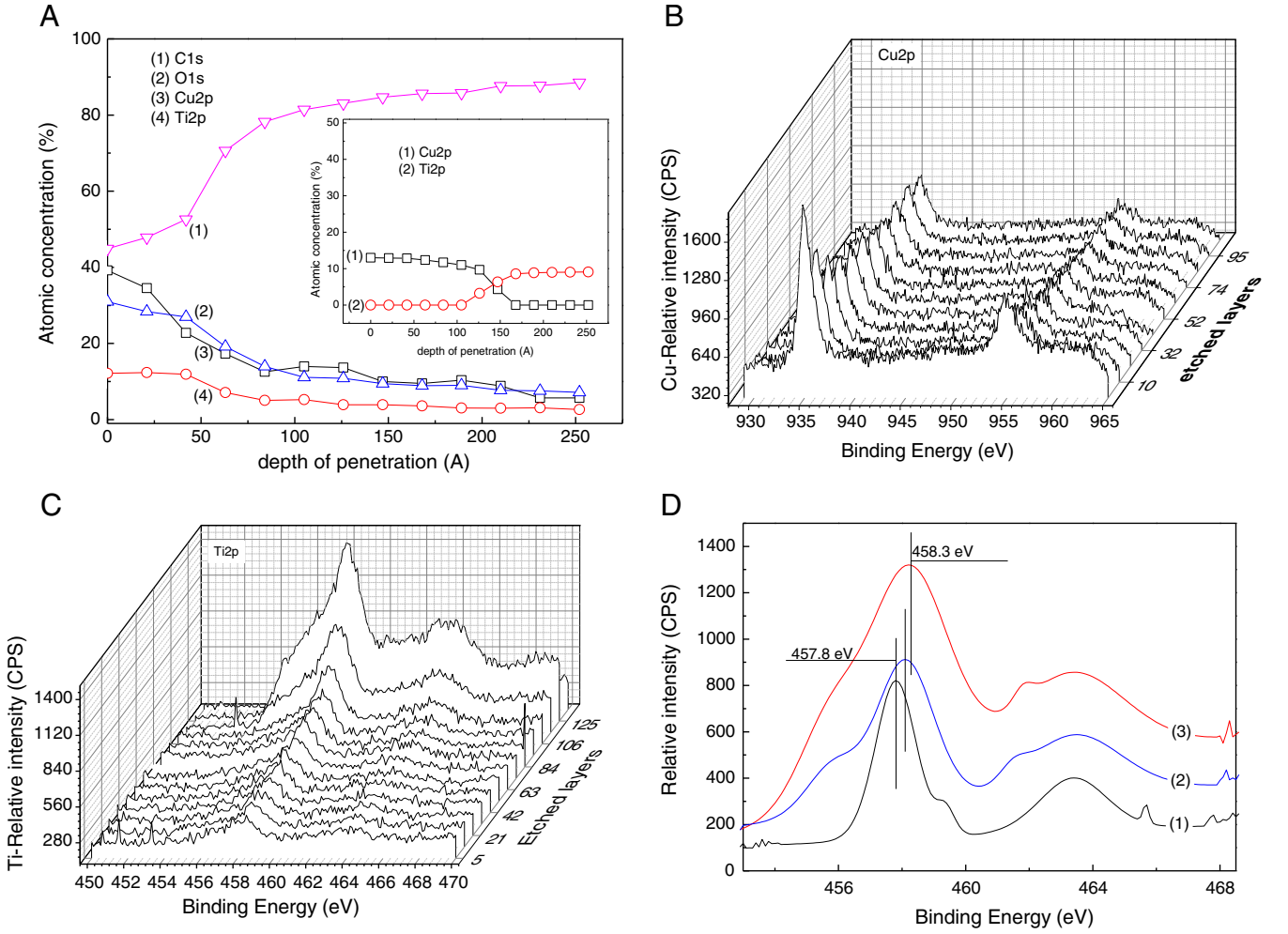

Fig. 3. A. XPS etching showing the microstructure of TiO_2/Cu film sputtered by HIPIMS up to 240 Å (~120 atomic layers). Inset: depth profile of the TiO_2/Cu film sputtered by DC/DCP. B. Depth profile of an Ar-etched TiO_2/Cu HIPIMS sputtered sample showing the Cu penetration in the film. C. Depth profile of an Ar-etched TiO_2/Cu HIPIMS sputtered sample showing the Ti penetration in the film. D. XPS Ti2p envelope changes at zero, 5 and 10 min during bacterial inactivation on TiO_2/Cu HIPIMS samples sputtered for 150 s under solar simulated light. E. XPS Ti2p deconvolution during bacterial inactivation with TiO_2/Cu HIPIMS sputtered for 150 s and irradiated by solar simulated light before and after bacterial inactivation. F. Cu2p XPS envelope at time zero, after 5 min and 15 min during bacterial inactivation on a TiO2/Cu sample sputtered for 150 s under solar simulated light. G. Cu2p peak deconvolution at time zero and 15 min after bacterial inactivation on a TiO_2 HIPIMS sputtered sample for 50 s under solar simulated light.

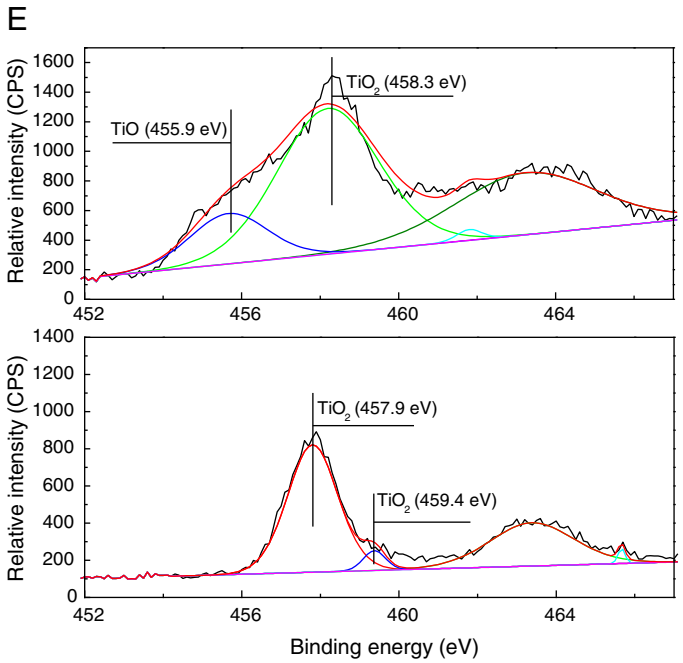

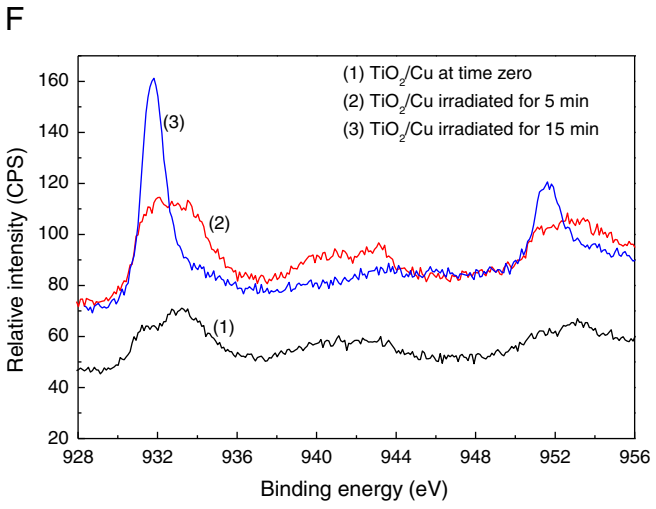

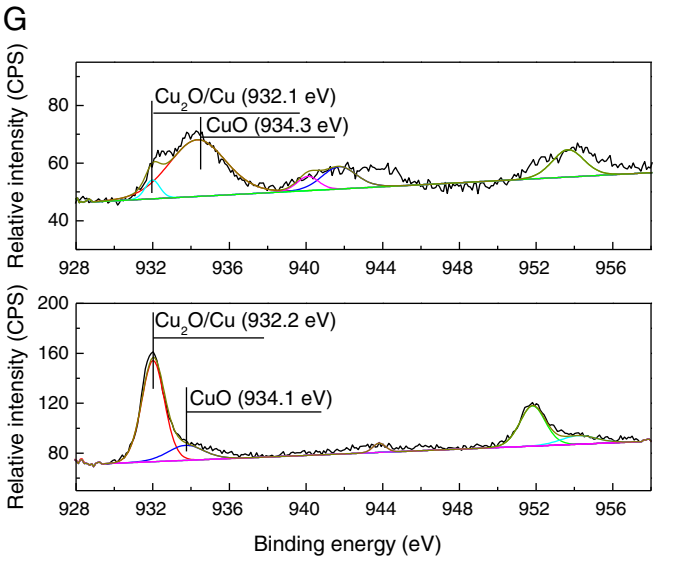

Fig. 3 (*continued*).

O. Due to its size, the CuO/Cu nanoparticles with particle size >8 nm are not able to penetrate into the bacteria core through the cell wall porins with diameters of 1–1.3 nm [25]. Only Cu-ions are able to diffuse through bacterial porins leading to DNA damage and finally to the total loss of bacterial viability.

Fig. 2C presents the XRD pattern for anatase and TiO_2/Cu were deposited on the HIPIMS samples sputtered for 30 s, 150 s and 300 s. The distinct pattern of the Cu peaks was not observed since the loading <0.1% was too low to be detected by XRD. The Cu/Cu_2O/CuO were deposited on the TiO_2 surface and did not lead to lattice doping. The TiO_2 sharp peak at 24.6° shows the highly crystallized TiO_2 sputtered on polyester.

3.3. X-ray photoelectron spectroscopy and Ar-etching of TiO_2/Cu films

The surface atomic percentage composition of C, O, N, S, Ti and Cu is shown in Table 2 as a function of bacterial inactivation time for HIPIMS sputtered samples up to 15 min. Table 2 shows a constant atomic percentage concentration implying that a rapid catalytic decomposition of the bacterial residues on the sample surface. Within 15 min the bacterial residues are destroyed enabling the catalyst recycling as shown in Fig. 1G.

Fig. 3A presents the atomic percentage concentration of Cu, Ti, O_2 and C of TiO_2/Cu samples sputtered for 150 s as a function of depth penetration of the Ar-ions. It is readily seen that Cu, Ti and O decrease up to 240 Å due to the Ar-bombardment. The etching depth induced by the Ar-ions was referenced by the known etching value for Ta of 15 atomic layers per minute equivalent to ~30 Å/min. The penetration of the Cu

Table 3
Surface atomic concentration percentage of CuO and Cu_2O on TiO_2/Cu HIPIMS sputtered for 150 irradiated by solar simulated light.

	% CuO	% Cu_2O
TiO_2/Cu at time zero	72	27
TiO_2/Cu at time of 15 min	18	80

inside the sample protects the Cu-clusters inside the 130 μm thick polyester network during the *E. coli* inactivation process. The increase in the C-content in Fig. 3A is due to the etching removing the TiO_2/Cu layers which make available the C-content of the polyester. The inset in Fig. 3A shows the significantly lower percentage of Cu and Ti for TiO_2/Cu sputtered by DC/DCP [17]. The concentration of Ti followed a different pattern compared to the one observed when sputtering by HIPIMS and increases beyond 100 Å because Ti deposition was hindered by the Cu-layers. Fig. 3B presents the 3-D view of the Cu 2p3/2 doublet and the Cu shake-up satellites at 933.4 eV and at 933.1 eV [18a] for the TiO_2/Cu 150 s HIPIMS sample. The Cu-enrichment within the 10 first layers is seen to decrease with sample depth and remain stable up to ~100 layers. Fig. 3C shows the Ti 2p3/2 doublet peaks with a binding energies (BE) at 458.5 and 464.1 eV, increasing steadily as we go deeper into the TiO_2/Cu film up to ~125 layers.

Fig. 3D presents the XPS envelope for the Ti2p signals at zero, 5 min and 10 min shown in the traces (1) through (3). It is readily seen that redox Ti^{3+}/Ti^{4+} processes take place during bacterial inactivation shifting the peak from 457.8 to 458.3 eV. This is >0.2 eV accepted as a true change in the oxidation state of a specific species [15,18a]. Fig. 3E presents the deconvolution of the peaks for the Ti2p doublet before and after the bacterial inactivation process. Evidence is presented for the reduction from Ti(IV) to Ti(III) in Fig. 3 by the shift of the deconvoluted peak from 457.9 eV at time zero to 458.3 eV after 10 min, the end of the bacterial inactivation.

Evidence is presented in Fig. 3F–G by XPS for Cu-redox chemistry during the bacterial inactivation in addition to the redox chemistry described above in Fig. 3D and e for Ti^{3+}/Ti^{4+} states. Fig. 3F at time zero presents the experimental envelope for the XPS peaks at time zero at 934.3 eV for CuO and at 932.1 eV for Cu_2O. The Cu_2O peak in TiO_2/Cu in Fig. 3F grows during the bacterial inactivation after 5 min and after 15 min when the bacterial inactivation is complete. In agreement with Table 3 a significant growth of the Cu_2O peak is detected in Fig. 3G due to two reasons: a) the CuO initial decreases from 72% to 18% while concomitantly the Cu_2O grows from 27% to 80% in line with the redox catalysis taking place in TiO_2/Cu shifting the CuO peak in Fig. 3G to CuO 934.1 eV and b) the bacteria covering initially the TiO_2/Cu catalyst have been removed during the inactivation process. It can be suggested that the interactions between Cu^+/Cu^{2+} and Ti^{3+}/Ti^{4+} in the TiO_2/Cu samples plays an active role accelerating the bacterial inactivation. The Ti^{3+}/Ti^{4+} surface electron trappers enhance the O_2 chemisorption at the surface more markedly in the TiO_2/Cu samples. This leads to a fast bacterial inactivation by TiO_2/Cu compared to Cu in Fig. 1D. The hole transition from TiO_2vb to the Cu mid band-gap states is in a second stage followed by indirect electronic transitions from the mid-gap states reaching the TiO_2cb.

3.4. Mechanism of the bacteria inactivation under visible light

Fig. 4A shows the interfacial charge transfer between TiO_2 and Cu in the TiO_2/Cu photocatalyst TiO_2/Cu under simulated solar irradiation. In the TiO_2 semiconductor the solar irradiation induces both the e^- transfer and h^+ transfer from TiO_2 to CuO since the potential energy levels of the TiO_2cb and TiO_2vb lie above the CuOcb and CuOvb levels. The partial recombination of e^-/h^+ in the TiO_2 is hindered by the transfer of charges to the CuO facilitating the reactions occurring at the TiO_2cb and CuOcb as shown in Fig. 4A. Under simulated solar light as shown in Fig. 4A, the CuO can be reduced to Cu_2O and the Cu_2O can reduce O_2 via a multi-electron process and re-oxidize to CuO. The charges generated by light in the TiO_2/Cu lead to the rapid loss of *E. coli* viability within 10 min (Fig. 1B), along O_2 and CuO reduction at the CuOcb as suggested in Fig. 4A.

The interfacial charge transfer (IFCT) in the TiO_2/Cu sample seems to proceed with a high quantum efficiency since the bacterial inactivation proceeds within short times of about 10 min (Fig. 1B). But the magnitude of the increase in the IFCT absorption of the TiO_2/Cu shown by the DRS spectra in Fig. 1E is relatively small.

The conduction band of CuO at −0.30 V vs SCE (pH 7) is at a more negative potential than the potential required for the one electron oxygen reduction $O_2 + H^+ + e^- \rightarrow HO_2^\circ$ −0.22 V [25,26]. Furthermore, the Cu^{2+} can react with e^- (or O_2^-) → Cu^+ + (or O_2). The Cu^+ can reduce O_2 consuming electrons or be oxidized to Cu-ions by the photo-generated TiO_2 holes to Cu^{2+} [27]. The TiO_2vb holes react with the surface −OH of the TiO_2 releasing OH-radicals to inactivate bacteria [28].

Fig. 4B presents the increase in fluorescence of the TiO_2/Cu HIPIMS sputtered samples irradiating up to 15 min in the solar simulator. The OH-radicals originate from the reaction between the OH-radical and terephthalic acid leading to the formation of a fluorescent hydroxy-product [19]. The TiO_2vb holes in Fig. 4A have the potential to degrade polyester during the bacterial inactivation cycles. But the stable repetitive *E. coli* loss of viability reported in Fig. 1G shows that bacterial inactivation did not lead to the degradation of polyester up to the 8th recycling.

3.5. DCP and HIPIMS sputtering of samples, applied power, charge density and bias voltage considerations

Fig. 5A presents the loss of viability time vs thickness for DCP and HIPIMS TiO_2/Cu sputtered films. Fig. 5A shows the much thinner TiO_2/Cu layer thickness necessary for complete bacterial inactivation sputtered by HIPIMS compared to DC/DCP. Fig. 5A shows that the HIPIMS film with a thickness of 38 nm inactivated bacteria within ~10 min compared to a sputtered DC/DCP film 600 nm thick inducing bacterial inactivation within the same period of time.

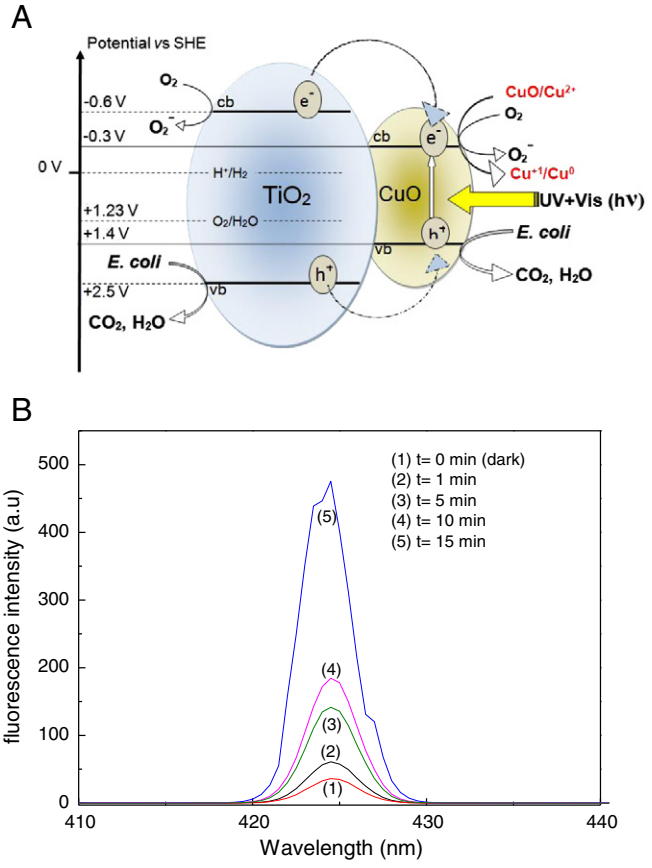

Fig. 4. Scheme of bacteria inactivation under visible light for TiO_2/Cu films on polyester. B. Fluorescence intensity as a function of irradiation time for HIPIMS sputtered 150 s samples on polyester irradiated by an Osram Lumilux 18 W/827 lamp.

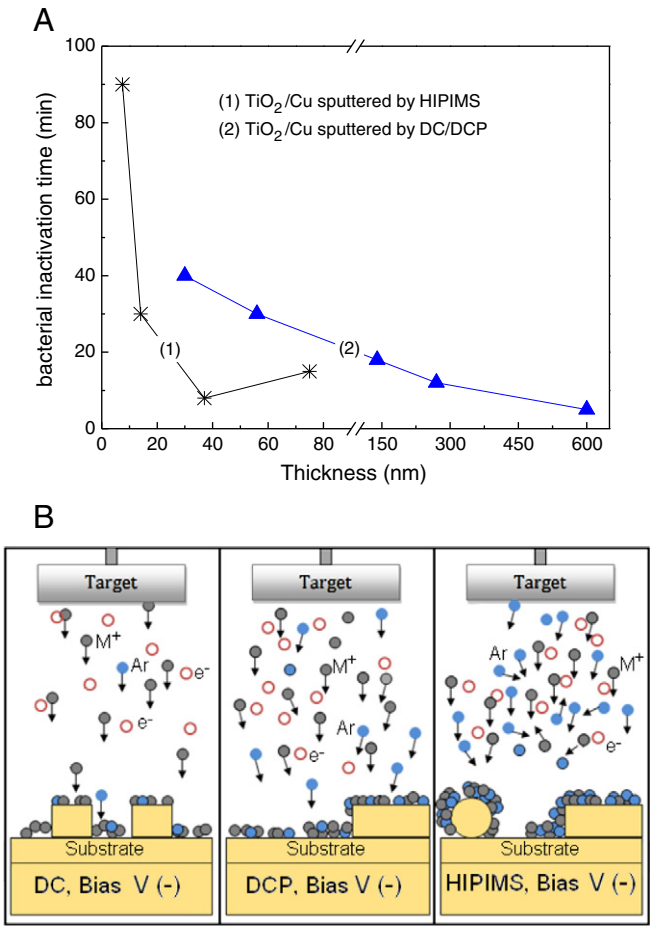

Fig. 5. A. Bacterial inactivation time vs nominal thicknesses for HIPIMS sputtered TiO_2/Cu films and by DC/DCP sputtered layers under Osram Lumilux 18 W/827 actinic lamp (4 mW/cm^2) irradiation. B. Schematics of the a) DC, b) DCP and c) HIPIMS sputtering of metal-ions (M^+) on polyester 3-D surfaces. For other details see text.

In Fig. 5B, the left hand side presents a scheme for the DC sputtering proceeding with an ionization of the Cu-ions of 1% [29]. The DCP sputtering is schematically presented in Fig. 5B (middle section) and proceeds with ionization of Cu-ions well above the values attained by DC [30]. In Fig. 5B, the right hand side involves HIPIMS sputtering leading to a Cu-ionization of ca. 70% and an electronic density of ~10^{18-19} e^-/m^3 [31]. The HIPIMS power per pulse was 1750 W/100 μs. This value is significantly higher than the power per pulse applied by DCP of 62.3 W/10 μs. The HIPIMS higher energy increased the ionization percentage $Cu^\circ \rightarrow Cu^+/Cu^{2+}$.

This increased arrival energy of the Cu-ions on the substrate allows the alignment of the Cu-ions on the polyester irregular (rugous) surface enabling a uniform coverage of the 3-D polyester [32]. The polyester 3-D presents that rugosity could not be quantified by atomic force microscopy (AFM) since it is beyond the AFM experimental range of 10 μm.

4. Conclusions

This study presents the first evidence for the surface functionalization of polyester by very thin HIPIMS layers of TiO_2/Cu able to inactivate bacteria in the minute range on 3-D surfaces like polyester fabrics. The TiO_2/Cu thin films were uniform, presented adhesive properties and led to repetitive loss of bacteria viability. A faster inactivation kinetics was observed by the TiO_2/Cu films compared to Cu or TiO_2 sputtered separately. A polyester sample HIPIMS sputtered for 10 min at 5 A led to a complete inactivation within 10 min under solar simulated light irradiation.

A considerable saving in metal and deposition time (energy) was found with HIPIMS compared to conventional DC/DCP-sputtering on 3-D surfaces. Increasing demand for Cu decreases rapidly the known world reserves. This is important since Cu is a strategically important metal. HIPIMS films of TiO_2/Cu and Cu on polyester have been shown in this study to preclude biofilm formation in the dark and more significantly under light irradiation.

Acknowledgments

We thank the COST Action MP 0804 and Dr R. Bandorf for the help with the HIPIMS experiments and the COST Action MP-1106 for interactive discussions. We also thank the financial support by the EPFL and the LIMPID FEP-7 Collaborative European Project Nanocomposite Materials for Photocatalytic Degradation of Pollutants NMP 2012.2.2.2-6 (n.310177).

References

[1] K. Taylor, R. Roberts, J. Roberts, J., The Challenge of Hospital Acquired Infections (HAI), Nat. Audit Office, 2002.
[2] S. Dance, J. Hosp. Infect. 73 (2007) 378–389.
[3] G. Borkow, J. Gabbay, J. FASEB 188 (2008) 1728–1730.
[4] A. Torres, C. Ruales, C. Pulgarin, A. Aimable, P. Bowen, J. Kiwi, *Appl.* Mater, Interf 2 (2010) 2547–2552.
[5] L. Zhang, R. Dillert, D. Bahnemann, Energy Environ. Sci. 5 (2012) 7491–7507.
[6] a K. Sunada, Watanabe, K. Hashimoto, Environ. Sci. Technol. 37 (2003) 4785–4789;
b O. Akhavan, R. Azimiriad, S. Safa, E. Hasani, J. Chem. Mater. 21 (2011) 9634–9640;
c O. Akhavan, E. Ghaderi, J. Chem. Mater. 21 (2011) 12935–12940;
d O. Akhavan, E. Ghaderi, Surf. Coat. Technol. 205 (2010) 219–223;
e M. Paschoalino, N.C. Guedes, W. Jardim, E. Mielczarski, J. Mielczarski, P. Bowen, J. Kiwi, J. Photochem. Photobiol. A 199 (2008) 105–111;
f M. Heinlaan, I. Blinova, H.-C. Dubourguier, A. Kahru, Chemosphere 71 (2008) 1308–1316;
g I. Perelshtein, G. Applerot, N. Perkas, E. Wehrschuetz-Sigl, A. Hasmann, G. Guebitz, A. Gedanken, Surf. Coat. Technol. 204 (2009) 54–57;
h L. Esteban-Tejeda, F. Malpartida, A. Esteban-Cubillo, C. Pecharromán, J.S. Moya, Nanotechnology 20 (2009) 505701;
i F. Gao, P. Huan, X. Shuoping, L. Qingyi, Chem. Commun. (2009) 3571–3573.
[7] H. Irie, S. Miura, K. Kamiya, K. Hashimoto, Chem. Phys. Lett. 457 (2008) 202–205.
[8] K. Page, M. Wilson, P.I. Parkin, J. Mater. Chem. 1 (2009) 3819–3831.
[9] H.A. Foster, P. Sheel, W.D. Sheel, P. Evans, S. Varghese, N. Rutschke, M.H. Yates, J. Photochem. Photobiol. A 216 (2010) 283–289.
[10] M.S.P. Dunlop, P.C. Sheeran, A.J.M. Byrne, S.A. McMahon, M.A. Boyle, G.K. McGuigan, J. Photochem. Photobiol. A 216 (2010) 303–3010.
[11] M.H. Yates, A.L. Brook, B.I. Ditta, P. Evans, H.A. Foster, D.W. Sheel, A. Steele, J. Photochem. Photobiol. A 197 (2008) 197–2008.
[12] J. Lin, J. Moore, W. Sproul, B. Mishra, Z. Wu, L. Wang, Surf. Coat. Technol. 204 (2010) 2230–2239.
[13] K. Sarakinos, J. Alami, D. Konstantinidis, Surf. Coat. Technol. 204 (2010) 1661–1684.
[14] P. Osorio, R. Sanjines, C. Ruales, C. Castro, C. Pulgarin, J.-A. Rengifo, J.-C. Lavanchy, J. Kiwi, J. Photochem. Photobiol. A 220 (2011) 70–76.
[15] E. Kusiak-Nejman, A. Morawski, A. Ehiasarian, O. Baghriche, C. Pulgarin, E. Mielczarski, J. Mielczarski, A. Kulik, J. Kiwi, J. Phys. Chem. C 115 (2011) 21113–21119.
[16] O. Baghriche, S. Rtimi, C. Pulgarin, T. Roussel, J. Kiwi, J. Photochem. Photobiol. A 213 (2013) 50–59.
[17] a) S. Rtimi, O. Baghriche, C. Pulgarin, R. Sanjines, J. Kiwi, ACS Appl. Mater. Interf. 4 (2012) 5234–5240;
b) L. Rio, E. Kusiak, J. Kiwi, C. Pulgarin, A. Trampuz, A. Bizzini, J. Appl. Microb. 78 (2012) 8176–8182.
[18] a) In: D. Wagner, M. Riggs, E. Davis, G. Müllenberg (Eds.), Handbook of X-ray Photoelectron Spectroscopy, Perkin-Elmer Corporation Physical Electronics Division, Minnesota, 1979;
b) D. Shirley, Phys. Rev. B5 (1972) 4709–4716.
[19] K. Ishibashi, A. Fujishima, T. Watanabe, K. Hashimoto, Electrochem. Commun. 2 (2000) 207–2010.
[20] W. Tung, W. Daoud, J. Mater. Chem. 21 (2011) 7858–7869.
[21] I. Mathews, Epitaxial Growth Part B, IBM, Academic Press, New York, 1975. 382–436.
[22] K. Hardee, A. Bard, J. Electrochem. Soc. 124 (1977) 215–224.
[23] V. Nadtochenko, V. Denisov, O. Savinov, J. Kiwi, J. Photochem. Photobiol. A 181 (2006) 401–407.
[24] J. Kiwi, C. Morrison, J. Phys. Chem. 88 (1984) 6146–6172.
[25] J.H. Nikaido, Biol. Chem. 269 (1994) 3905–3909.

[26] A. Nozik, Annu. Rev. Phys. Chem. 2 (1978) 189–222.
[27] J. Bandara, I. Guasaquillo, P. Bowen, L. Soare, W.-F. Jardim, J. Kiwi, Langmuir 21 (2005) 8554–8559.
[28] D. Ward, A. Bard, J. Phys. Chem. 86 (2004) 3599–3604.
[29] Petrov, A. Myers, J.E. Greene, J.R. Abelson, J. Vac. Sci. Technol. A 12 (1994) 2846–2851.
[30] J. Alami, P. Persson, J. Gudmunsoon, J. Bohlmark, J. Helmersson, J. Vac. Technol. A 23 (2005) 278–280.
[31] V. Kousznetsov, K. Macak, J. Schneider, U. Helmersson, I. Petrov, Surf. Coat. Technol. 12 (1999) 290–295.
[32] S. Rossnagel, J. Hopwood, J. Appl. Phys. Lett. 63 (1993) 32–34.